The Cryosphere Discuss., https://doi.org/10.5194/tc-2019-81
Manuscript under review for journal The Cryosphere
Discussion started: 23 May 2019

The Cryosphere Discussions
Open Access
EGU

Assessing the performance of a distributed radiation-temperature melt model on an Arctic glacier using UAV data

Eleanor A. Bash[1] and Brian J. Moorman[1]

[1]Department of Geography, University of Calgary, Calgary, Alberta, Canada

Correspondence: Eleanor A. Bash (eleanor.bash@gmail.com)

Abstract. Enhanced temperature index (ETI) models of glacier surface melt are commonly used in studies of glacier mass balance and runoff. With limited data available most models are validated based on ablation stakes and data from automatic weather stations (AWS). With the technological advances of unmanned aerial vehicles (UAVs) and structure-from-motion (SfM), it is possible to measure glacier surface melt in detail over larger portions of a glacier. In this study, we use melt measured using SfM processing of UAV imagery to assess the performance of an ETI melt model in two-dimensions. Imagery collected over a portion of the ablation zone of Fountain Glacier, NU, on July 21 and 24, 2016 was previously used to determine distributed surface melt. Incoming solar radiation and temperature measured at the AWS, along with albedo derived from UAV imagery, are used as inputs for the model which was used to estimate melt from July 21-24, 2016. Modelled melt agrees with melt measured at the AWS within ±0.010 m. Across the study area the median model error (-0.044 m), calculated as the difference between measured and modelled melt, is within the uncertainty of the measurements. A strong link was found between the model error and glacier surface aspect with higher errors linked to south aspects. The highest errors were also linked to the density of water flow features on the glacier surface. The relation between water flow and model error suggests that energy from surface water flow is contributing significantly to surface melt on Fountain Glacier. Deep surface streams with highly asymmetrical banks are observed on Fountain Glacier, but the processes leading to their formation are missing in the model assessed here. The failure of the model to capture flow-induced melt and to under-estimate melt on south aspects would lead to significant underestimation of surface melt should the model be used to project future change.

1 Introduction

The Canadian Arctic Archipelago holds approximately 14% of the world's glacier ice outside the major ice sheets (Gardner et al., 2011). Rates of glacier melt in the Canadian Arctic have increased since the late 1990s (Noël et al., 2018; Lenaerts et al., 2013; Gardner et al., 2012). Fisher et al. (2012) show that recent melt rates on Canadian Arctic ice caps are the highest in 4000 years. Collectively, glaciers of the southern Canadian Arctic Archipelago contributed over 16% of 2003-2010 sea-level rise (Gardner et al., 2012). Future projections indicate the glaciers from across Arctic Canada will continue to be the largest

The Cryosphere Discuss., https://doi.org/10.5194/tc-2019-81
Manuscript under review for journal The Cryosphere
Discussion started: 23 May 2019

mountain glacier contributors to sea-level rise through the end of this century (Radić and Hock, 2011). Given the importance of Canadian Arctic glaciers to global sea-level rise and the rapid change in melt rates observed in recent years, it is critical to better understand the processes contributing to melt rates on these glaciers.

Direct measurements of melt rates on Arctic glaciers are scarce, only five glaciers from the Canadian Arctic have current data available online (WGMS, 2018). Where in situ data is collected, it is often based on ablation stake networks and data from automatic weather stations (AWS) (e.g. Bash et al., 2018; WGMS, 2018). These in situ measurements must be extrapolated to provide estimates of melt at other locations on a glacier, or at other glaciers where no measurements exist. Several kinds of models are commonly used to extrapolate glacier surface melt measurements, including temperature index (TI), enhanced temperature index (ETI), and energy balance (e.g. Hock, 1999, 2005; MacDougall and Flowers, 2011; Irvine-Fynn et al., 2014; Bash and Marshall, 2014; Shaw et al., 2016). The TI or ETI models are often preferred for regional scale models, because of their lower computational needs and the ease with which input variables can be estimated.

Validating model results is also difficult due to the lack of data available on Arctic glaciers. Datasets are often split into training and validation periods to assess model performance. Available measurements represent only a few locations on the glacier surface, however (Mair et al., 2003; Wake and Marshall, 2015; Matthews et al., 2015). Where outlet streams are measured, studies use total stream discharge and aggregated surface melt to validate results (e.g. Pellicciotti et al., 2005; Bash and Marshall, 2014). Validation with total melt provides insight into the average performance of these models over an entire glacier, but neither this method or the validation based on point data provide insight into model performance across a glacier surface.

Technological advances have allowed for increasingly detailed change detection from imagery obtained by satellites, unmanned aerial vehicles (UAVs), and terrestrial photography. Structure-from-motion (SfM) is widely used across a range of disciplines for reconstructing topography using imagery from the aforementioned sources (e.g. James and Robson, 2014; Cook, 2017; Watson et al., 2017; Lovitt et al., 2018; Bash et al., 2018). Employing SfM, Watson et al. (2017) use multiple reconstructions of a debris covered glacier to measure seasonal ice cliff retreat from terrestrial photographs, including spatial variation in rates across individual cliff faces. Using similar methods and UAV imagery, Bash et al. (2018) measure spatially variable melt rates in the ablation zone of an Arctic glacier over 3 days. This new capacity for measuring change in great temporal and spatial detail provides opportunities to examine spatial patterns in ways that were previously not possible.

The methods of surveying that are needed for detailed surface change measurements using SfM are time consuming (Watson et al., 2017; Bash et al., 2018; Avanzi et al., 2018). These surveys involve multiple site visits, measurement of control points using differential GPS or total stations, and imagery collection (Bash et al., 2018). Given the effort involved in these data collection campaigns, it is not feasible at this time to extend these methods to regional-scale glacier change detection. Modelling efforts will continue to play an important role in understanding glacier melt in the future and thus it is critical to improve the models employed.

The aim of this study is to use melt measurements available in high spatial and temporal resolution to assess the performance of an ETI model across the glacier surface. We do this using previously published surface melt data which was measured using UAV surveys in the ablation zone of Fountain Glacier, NU (Bash et al., 2018).

The Cryosphere Discuss., https://doi.org/10.5194/tc-2019-81
Manuscript under review for journal The Cryosphere
Discussion started: 23 May 2019

2 Methods

2.1 Study Area

Fountain Glacier, located on Bylot Island, NU (Figure 1), has been studied in detail since 1991 (e.g. Moorman, 2003; Whitehead et al., 2014; Bash et al., 2018). The glacier stretches 16 km from higher elevations in the Byam Martin Mountain Range to its terminus roughly 10 km inland from the coast. The focus area of this study, in the lower ablation zone, spans a narrow elevation range (250–400 m) and terminates in a cliff face with two calving fronts. The lower portion of the glacier faces east, with several supraglacial streams of varying sizes (St. Germain and Moorman, 2016). The largest of these streams form deeply incised asymmetrical canyons, with a steeper north facing valley wall and a more gently sloping south facing valley wall (Figure 1).

During July of 2016 aerial surveys were conducted with a UAV to reconstruct the surface multiple times (Bash et al., 2018). Bash et al. (2018) measured surface lowering between July 21 and 24 using point cloud differencing across the study area indicated in Figure 1. Concurrently, an automatic weather station (AWS; Figure 1) was recording surface melt, as well as temperature, incoming and outgoing shortwave radiation, relative humidity, wind speed and direction. Bash et al. (2018) assessed the surface lowering against 17 ablation stakes, as well as the AWS data, and found that the surface lowering measured through point cloud differencing agreed with melt measurements throughout the study area. The root mean square error (RMSE) of the measured surface lowering at the ablation stakes was 0.048 m.

Bash et al. (2018) measured an average daily melt rate of 6.0 cm day^{-1} across the study area between July 21-24, 2016. Average melt rates of 3.0–5.5 cm day^{-1} were found by Whitehead et al. (2014) in summer 2010–2011. Bash et al. (2018) also showed, however, that melt was highly variable across the study area during that time ranging from 1.0–11.0 cm day^{-1}. The authors found that these differences in melt were not tied to elevation or aspect of the glacier surface.

2.2 Description of Data

All AWS measurements were taken at 2 min intervals and recorded as hourly averages from July 13 to August 2, 2016 (Figure 2A, 2D, 2E). An SR50 sonic ranger was installed on a pole drilled into the glacier surface immediately next to the AWS and measured hourly average surface position for the same time period. The pole holding the SR50 began to tilt due to melt out of the pole during the afternoon of July 27 and was reinstalled in the morning on July 28. The data from that time period was removed from the time series (Figure 2).

Models run at high temporal resolution can have significant errors which stem from SR50 readings (Matthews et al., 2015). These errors stem from the uncertainty in SR50 readings due to the instrument accuracy (0.01 m), as well as uneven topography underneath the instrument. In addition to hourly surface position the SR50 records a standard deviation of all measurements in the hourly average (typically 30). SR50 values where the standard deviation was greater than 0.01 m were removed and then a 5 hr rolling average was calculated. SR50 values which differed significantly from others in the 5 hr window were also removed. Melt was then calculated in 12 hr periods (0:00 – 12:00) using the remaining values.

The Cryosphere Discuss., https://doi.org/10.5194/tc-2019-81
Manuscript under review for journal The Cryosphere
Discussion started: 23 May 2019

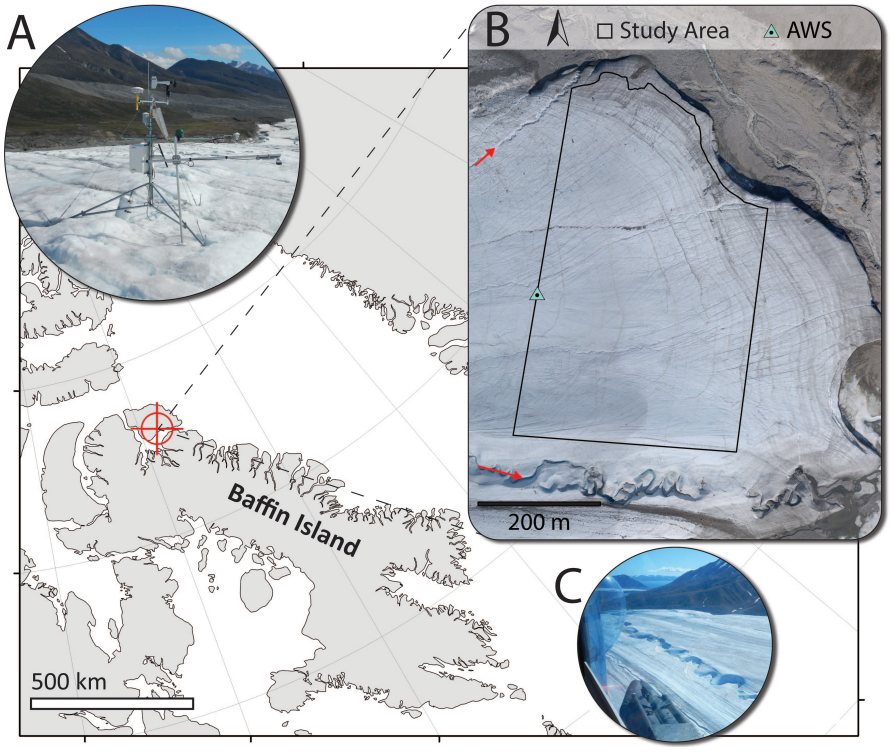

Figure 1. Location of Fountain Glacier on Bylot Island, NU, in the Canadian Arctic. (**A**) The automatic weather station (AWS) installed on a tripod, measuring incoming and outgoing shortwave radiation and temperature. An SR50 measuring surface position was installed on a separate pole drilled into the glacier (foreground). (**B**) A 2011 orthomosaic of the lower ablation zone of Fountain Glacier. The boundary of the study area is shown, the area extends to the 2016 glacier boundary on the north side. The AWS location is also indicated (green triangle). Two canyons formed by stream incision are indicated in red. (**C**) An aerial view of the largest incised canyon on Fountain Glacier. The photo is taken facing east and the steep north facing canyon walls can be seen in contrast to the more gently sloping south facing walls.

Processing of UAV imagery was done in Agisoft Photoscan and is described in detail by Bash et al. (2018). During processing, point clouds of the glacier surface at mid-day were produced for July 21 and 24, 2016. The point clouds were used to create orthomosaics and digital surface models (DSM) for each day with resolutions of 0.10 m.

The multiscale model to model cloud comparison algorithm (M3C2) was used to calculate melt across the study area at 0.02 m resolution (Lague et al., 2013; Bash et al., 2018), with uncertainty of 0.048 m based on the RMSE at ablation stakes. To align with DSMs and orthomsaics of the study area, for this study melt data was gridded to 0.10 m resolution. Melt measurements were averaged within each grid cell and empty cells were filled using bilinear interpolation.

The Cryosphere Discuss., https://doi.org/10.5194/tc-2019-81
Manuscript under review for journal The Cryosphere
Discussion started: 23 May 2019

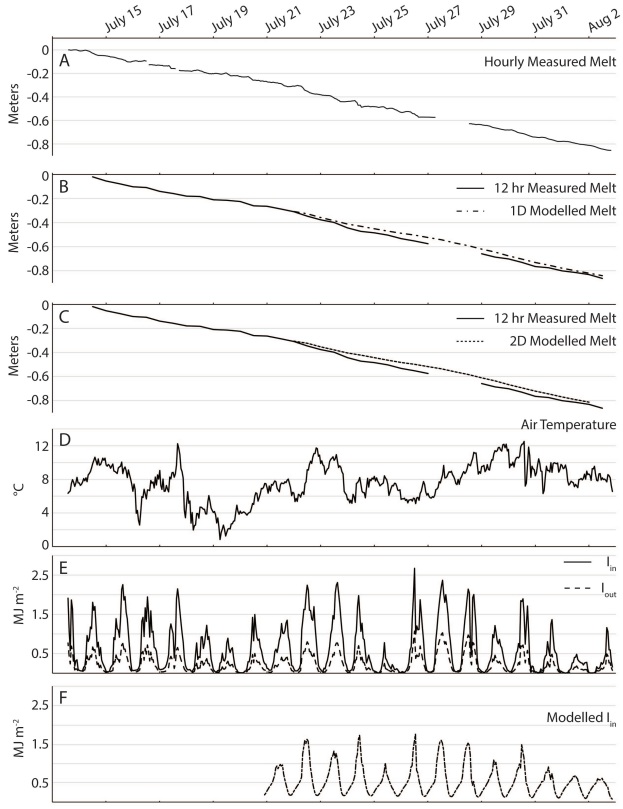

Figure 2. Measured and modelled melt, as well as input variables, for the period July 13 – August 2. A gap exists in measured melt due to melt out of the pole holding the SR50. Melt was extrapolated during this time for better visual comparison, extrapolation was based on average melt rates for the day prior to and following the gap. A) Surface change measured hourly at the AWS. (**B**) Twelve hour melt totals measured at the AWS and modelled with AWS data. (**C**) Twelve hour melt totals measured at the AWS and modelled with distributed variables. Modelled melt estimates were extracted from the output cell containing the AWS. (**D**) Hourly average measured near surface air temperature. (**E**) Hourly average incoming (I_{in}) and outgoing (I_{out}) shortwave radiation measured at the AWS. F) Hourly incoming shortwave radiation modelled based on DSM slope and aspect, measured Iin, and a parametrization of diffuse radiation. Modelled radiation values were extracted from the output cell containing the AWS.

2.3 Model Formulation

This study assesses the performance of an enhanced temperature index model because these models are commonly used for regional scale estimations of glacier melt. The model we use is formulated after Bash and Marshall (2014), which uses absorbed radiation (I_{abs}) and temperature (T) in a linear regression model to estimate melt (M). The formulation of the model is unique

The Cryosphere Discuss., https://doi.org/10.5194/tc-2019-81
Manuscript under review for journal The Cryosphere
Discussion started: 23 May 2019

in that it controls for correlation between independent variables which can make model results unstable when not addressed. The uncorrelated temperature ($T_{residual}$) is calculated by:

$$T_I = \eta + \beta I_{abs} \qquad T_{residual} = T - T_I \tag{1}$$

Where η and β are coefficients fit using a linear regression. $T_{residual}$ is then used in the following equation to determine melt:

$$\hat{M} = \begin{cases} TF \cdot T_{residual} + RF \cdot I_{abs} & : T > 0 \\ 0 & : T \leq 0 \end{cases} \tag{2}$$

where I_{abs} can be calculated by the difference between incoming and outgoing radiation, or by multiplying incoming radiation by $(1-\alpha)$, where α is the surface albedo. TF and RF are coefficients fit using a linear regression.

Cumulative positive $T_{residual}$ and I_{abs} were calculated for 12 hr periods beginning July 14 at 12:00. Data from July 14 – July 20 was used to determine the model coefficients (η, β, TF, RF) using a multiple linear regression. The model will estimate no melt if actual air temperature falls below zero, but temperatures remained above zero through the study period.

To distribute the model across the study area input variables need to be estimated for each grid cell. Given the relatively small size of the study area and elevation range of only 150 m, temperature was assumed to remain constant across the area. Radiation estimates varied however, described below, and thus $T_{residual}$ also varied across the area.

Distributed incoming radiation was calculated by modifying the hourly measured incoming radiation at the AWS by the slope and aspect of each grid cell (Figure 3C). The terrain correction was based on Goswami et al. (2000). This correction alone causes radiation to drop to zero overnight, which is not realistic during Arctic summers. Although direct radiation may drop to zero at some cells when sun angles are low overnight, diffuse radiation is at measurable levels (Figure 2E). A diffuse correction was made based on Bugler (1977) to estimate the total incoming radiation (Figure 2F). Lower peak radiation in the model is due to a slight difference in slope and aspect between the radiometer (which is level) and the grid cell of the DSM containing the AWS. Estimated radiation at each cell was then multiplied by $(1-\alpha)$ to estimate I_{abs} at each cell.

Albedo was estimated across the study area using the orthomosaics from July 21 and July 23. Each orthomosaic contains the digital number recorded by the camera in the red, green, and blue (RGB) channels. The digital number cannot be directly used to calculate surface reflectance without conversion equations propriety to the camera manufacturer. However, several studies have used other means to convert digital numbers to surface reflectance (Corripio, 2004; Rippin et al., 2015; Ryan et al., 2017), we employed an approach similar to that of Rippin et al. (2015).

Values for RGB channels were averaged and the total range scaled to a range of 0.55-0.1 (Figure 3). The upper end of the range was determined by the average surface albedo measured at the AWS during the study period, while the lower end was based on albedo values of cryoconite holes reported by Ryan et al. (2017). An assumption was made that cryoconite holes would have similar albedo to debris on the glacier surface. The scaling of RGB values was used to create a gridded albedo

The Cryosphere Discuss., https://doi.org/10.5194/tc-2019-81
Manuscript under review for journal The Cryosphere
Discussion started: 23 May 2019

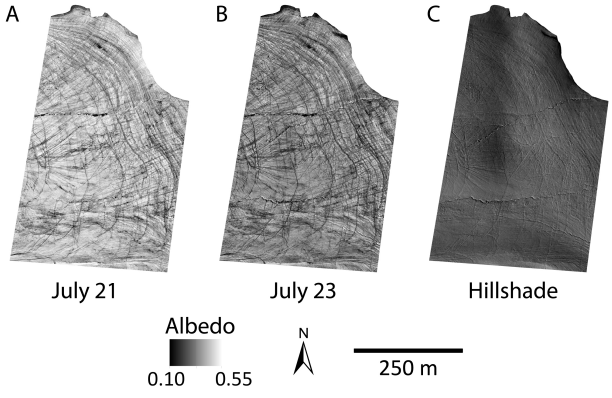

Figure 3. Albedo was derived from UAV imagery using an average values from RGB bands and scaling the lower and upper bounds to match the albedo of bare rocks (based on REF) and the average albedo measured on Fountain Glacier during the study period. (**A**) July 21 albedo values. (**B**) Juy 23 albedo values. (**C**) A hillshade model of the study area based on the DSM from July 21.

product that could be directly input into the melt model. July 21 albedo was used as a model input for 12:00 July 21 – 12:00 July 23, while the July 23 albedo was used from 12:00 July 23 onward.

2.4 Model Performance

The one-dimensional formulation of the model at the AWS (ETI_{AWS}) and the distributed model (ETI_{dist}) were both run for the period from 00:00 July 21 to 12:00 August 2, 2016. As described above, measured temperature and absorbed radiation were used as inputs for ETI_{AWS}. Measured temperature and modelled radiation were input to ETI_{dist}.

The results were compared to measured melt at the AWS to assess model performance. To compare ETI_{dist} estimates, melt values were extracted from the grid cell containing the AWS. Both models were assessed using the mean, standard deviation, and root mean square (RMS) of the residuals ($M - \hat{M}$).

Melt estimates for July 21–24 from ETI_{dist} were compared to measured melt across the study area for the same period. Model error was calculated at each grid cell in the study area. The median model error (ME) and normalized median absolute deviation (NMAD) were used to describe the model error following Höhle and Höhle (2009). The median and range of measured and modelled melt were also calculated for comparison.

In addition to model performance, the model error across the study area was used to investigate factors influencing model performance. We examined model errors in relationship to surface characteristics which are known to influence the energy available for melt (Hock, 2005). Correlations were computed between model error and terrain variables (slope and aspect), albedo, and an estimate of surface water flow.

Water flow was quantified using the Hydrology Toolset in ArcGIS 10. Assuming that water is produced at every grid cell flow paths were calculated from the DSM based on up-slope accumulation. Cells with more than 1500 upstream cells were converted to a set of linear features and the number of these features within 20 m of each grid cell was calculated (W_{20m}). The

The Cryosphere Discuss., https://doi.org/10.5194/tc-2019-81
Manuscript under review for journal The Cryosphere
Discussion started: 23 May 2019

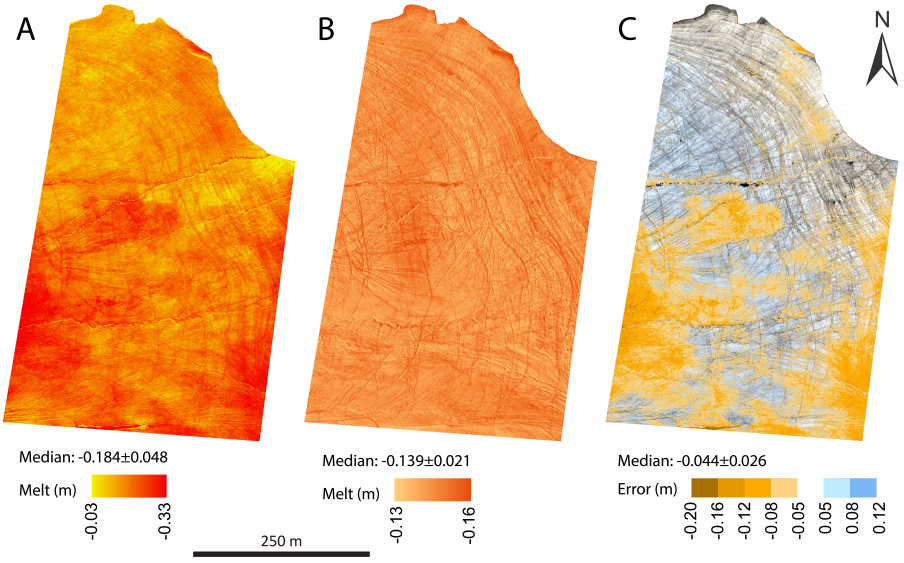

Figure 4. Distribution of measured and modelled melt across the study area. Different color scales are used in A and B due to drastic differences in the range of melt values between the two. (**A**) Melt measured through differencing surfaces reconstructed from UAV imagery. (**B**) Melt estimated using ETI_{dist} applied across the study area. The distributed model is run with measured radiation, adjusted based on slope and aspect at 10 cm resolution, and albedo derived from UAV imagery. (**C**) Model error, calculated by the difference between measured and modelled melt. Cells with an absolute value lower than the measurement error (0.048 m) are transparent to emphasize areas where the model performs poorly.

20 m radius was chosen to represent surface flow features observed in the field. The resulting layer provided a representation of areas with significant surface water flow, including streams and thin sheet flows.

3 Results

Melt estimated with ETI_{AWS} and ETI_{dist} during the validation period both performed well, but with notably lower variability than measurements (Figure 2B, C). The mean residual for ETI_{AWS} was -0.001 m, with standard deviation of 0.010 m, and RMS of 0.010 m. Performance of ETI_{dist} was similar, with a mean residual of 0.000 m, standard deviation of 0.010 m, and RMS of 0.011 m.

Across the study area median modelled melt was -0.139 m (Figure 4B), while median measured melt was -0.184 m (Figure 4A). Like the performance of ETI_{AWS}, ETI_{dist} shows significantly lower variability than measured melt. The range of ETI_{dist} across the study area was 0.028 m, while the range of measured melt was 0.305 m. Overall the ME was -0.044 m, with an NMAD of 0.026 m.

The Cryosphere Discuss., https://doi.org/10.5194/tc-2019-81
Manuscript under review for journal The Cryosphere
Discussion started: 23 May 2019

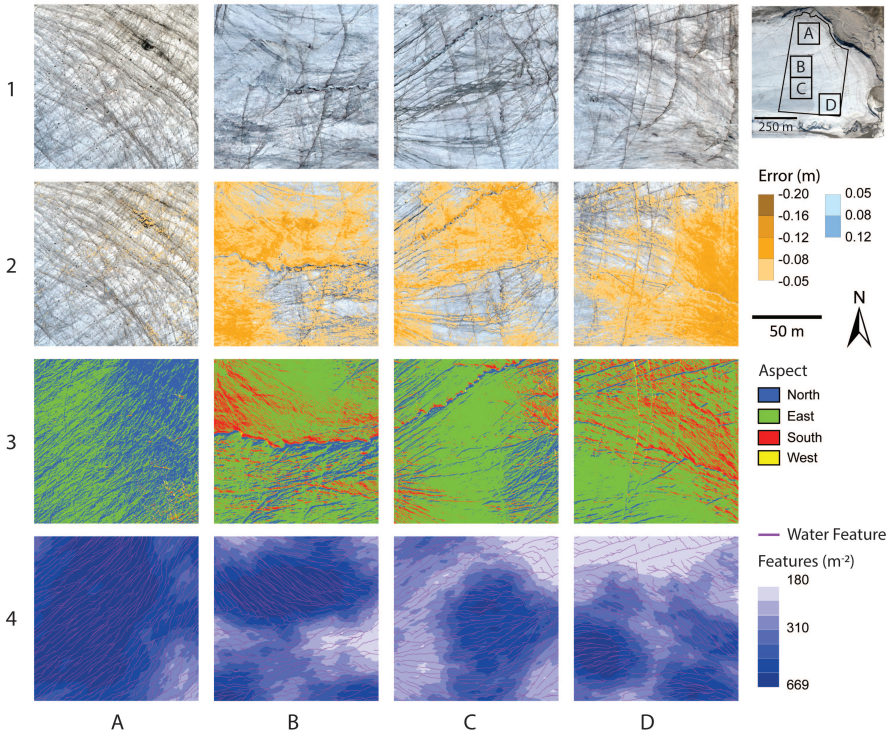

Figure 5. Four example locations showing model error, surface aspect, and density of water features. Extents of example locations (**A–D**) are shown in the inset map. Panels show the orthomosaic (**1**), model error (**2**), aspect (**3**), and water feature density overlain by water features (**4**). The strong relationship between surface aspect and model error can be seen in all four locations. In A2 model error is low, despite high stream feature density, due to predominantly north aspect. While in **B1-3**, **C1-3**, and **D1-3** areas of high error are associated with predominantly south aspects and high density of water features. In **B2-3** and **D2-3** west-east flowing streams have high errors on south aspect banks, and generally lower or minimal error on north facing banks. Areas of positive model error (**A2**) are found where large boulders are present on the glacier surface.

The ME is lower than the measurement uncertainty (0.048 m), indicating general agreement with measurements. When areas of error above the measurement uncertainty are highlighted (Figure 4C), they show clustered patterns representing 45% of the total study area. Errors greater than twice the uncertainty (0.096m) account for 5% of the study area.

A significant correlation ($p<0.05$) was found between model error and aspect, 0.34. Cells with south aspects had a mean error of -0.067 m, while those with north aspects had a mean error of -0.032 m. The relationship is visually apparent throughout the study area as well (Figure 5A2-D2, A3-D3), and is particularly notable along east-flowing supraglacial streams (Figure 5B2-3, D2-3). Statistically significant correlations were found with slope and albedo, but correlation values were much lower (<0.1), and thus were not investigated further.

The Cryosphere Discuss., https://doi.org/10.5194/tc-2019-81
Manuscript under review for journal The Cryosphere
Discussion started: 23 May 2019

Through field experience, we were able to note a visual relationship between surface water features and high error during analysis (Figure 5B1-D1, B2-D2). This association was confirmed through correlation with W_{20m} (Figure 5A4-D4). A significant correlation ($p<0.05$) was found between errors less than -0.048 and W_{20m}, 0.22.

Although most of the errors are negative, positive errors were also found. These are primarily associated with boulders and other large stationary objects on the glacier surface (Figure 5A2).

Model uncertainty can be derived from a number of metrics, including the results of ETI_{AWS} and ETI_{dist}. Using statistical measures, model uncertainty is often quantified by the variability in the errors represented by the RMS (0.011 m) and NMAD (0.026 m). However, in this case the 95th quantile of the errors (0.095 m) suggests this would be an underestimate. Bash and Marshall (2014) use validation at an AWS and incorporate uncertainties related to modelling input variables to estimate an uncertainty of 15%. In either case, the errors which are strongly correlated with surface aspect and W_{20m} are higher than the combined uncertainty of measurement and model. These combined errors may range from 0.049–0.11 m.

4 Discussion

The ETI models derived using data from the AWS performed well during the validation period of July 21–August 2, 2016. Both ETI_{AWS} and ETI_{dist} simulated melt at the location of the AWS to within 0.000±0.010 m per 12 hr period. For comparison to other studies, this was converted to a standard deviation of 0.00083 m h^{-1}. This performance is similar to other ETI models in the literature (Pellicciotti et al., 2005; Irvine-Fynn et al., 2014; Bash and Marshall, 2014). Irvine-Fynn et al. (2014) report a standard error of 0.00018 – 0.00053 m h^{-1}, the range in error stems from model runs with different training datasets. Hourly ETI model error reported by Pellicciotti et al. (2005) is as high as 0.0055 m water equivalent h^{-1}, compared to an energy balance model as reference data. Bash and Marshall (2014) report a standard error of 0.00031 m h^{-1}, when the model is validated against data from a different year. While our results show a higher standard deviation, it is important to note that the uncertainties associated with modelling input data are likely to outweigh the discrepancies between this and other studies, as noted by Bash and Marshall (2014); Pellicciotti et al. (2005). Overall these results at the AWS indicate that, in the absence of additional validation data, it would be reasonable to employ this model to estimate melt across the glacier surface.

Hock (1999) found that when TF is calculated based on melt and temperature records, it is highly variable. The inclusion of shortwave radiation in ETI models is an attempt to account for this variability. The low variability seen in the results of both ETI_{AWS} and ETI_{dist} when compared to AWS measurements is an indication of potential problems in the ETI models. Similar muted model estimations were noted in other studies (Hock, 1999; Bash and Marshall, 2014). However, Hock (1999), Pellicciotti et al. (2005), and Irvine-Fynn et al. (2014), all cite R^2 values of 0.60, 0.86, and 0.80 when comparing total modelled melt to measured discharge. These previous results show that although the ETI models capture total melt, melt rates at individual points are captured less effectively. Similarly, we found across the study area that median modelled and measured melt agreed, but model results showed variability an order of magnitude lower than measurements (Figure 4A, B). The availability of melt measurements at 10 cm resolution shed light on the areas where modelled and measured melt were (or were not) in agreement,

which has not been shown before. These measurements also allowed us to examine possible explanations for the model errors, including the aspect and surface water flow.

It is worth noting that surface lowering measured through point cloud differencing is not always equivalent to surface melt. Vertical ice motion in the ablation zone offset melt in measurements of surface change. However, in the case of Fountain Glacier Whitehead et al. (2014) estimate surface uplift to be 0.2 m over the course of the ablation season, or 0.002 m d^{-1}. Given the magnitude of measured surface elevation change over the 3 day period and the correspondence of those measurements to melt measured at ablation stakes, we assume that vertical uplift is a negligible contribution and the point cloud differences represent surface melt.

The eastern orientation of Fountain Glacier results in primarily east draining supraglacial streams with north and south facing banks (Figure 5B, D). Bash et al. (2018) noted clear differences in measured melt on north and south facing stream banks, which was not seen in ETI_{dist} results. These differences in melt on opposite banks lead to the asymmetrical shape of canyons found on Fountain Glacier. Correlation between aspect and ETI_{dist} error was significant. South facing grid cells had an average error nearly twice that of north facing cells, with less variability in that error. Much of the study area is east and south facing, Figures 5B and 5D show east-west oriented streams with higher error on south facing banks. The northern portion of the study area slopes northward and overall has lower error (Figure 4C, Figure 5A). Close agreement between ETI_{AWS} and ETI_{dist} at the AWS, indicates the relation between model error and aspect is unlikely to be an artefact of radiation modelling. The explanation for the correlation remains unclear.

Bash et al. (2018) measured melt rates within active supraglacial streams higher than rates of melt on the ice surrounding those streams. This higher rate of melt leads to streams downcutting into the glacier surface over time, as long as melt water routing paths remain constant. Bash et al. (2018) also noted the difference in melt rate between an active stream and the nearby channel which the stream formerly occupied. During preliminary analysis of ETI_{dist} results, we noted the occurrence of high model errors in areas with visual evidence of surface water flow including thin sheet flow and streams. Further investigation revealed correlation between density of linear flow features (designated through DSM analysis and representing streams as well as thin sheet flow) and model errors less than -0.048 m, with a slightly more pronounced correlation on south facing aspects. Figure 5A is an example of an area with predominantly north aspect, which exhibits high density of surface water features, but low model error. The relation between model underestimation and surface water features suggests the water flowing on the glacier surface is contributing a measurable amount to surface melt. This is consistent with observed patterns of downcutting streams and higher melt in active stream channels, but also shows the importance of water in areas with thin sheet flow over the glacier surface.

Stevens et al. (2018) note the role of kinetic energy in development of surface weathering crusts and the complexity of near-surface glacier hydrology which is only recently coming to light. Temperatures measured in a supraglacial stream on Fountain Glacier in 2014 ranged from 0-0.1°C (St. Germain and Moorman, 2016). These temperatures alone are not sufficient to explain the magnitude of model errors in the vicinity of water features, suggesting that other forms of energy transfer are playing an important role. Idealized crevasse bottom incision equations presented by Fountain and Walder (1998) are driven by discharge rates, suggesting a role in flow related incision for both heat advection as well as energy transfer from kinetic and

potential energy. Irvine-Fynn et al. (2011) note that the relative importance of frictional heat contributing to incision rates in nontemperate glaciers remains unresolved.

The correlation of high model error with water feature density was significant in areas with thin sheet flow, in addition to the locations of supraglacial streams. The contribution of melt energy to the glacier surface from less concentrated water flow found here has not been examined in previous studies, and these results add new insight to the emerging picture of complex surface hydrology on nontemperate glaciers. The relatively lower correlation of model errors with water features on north aspects may be due to lower melt water production on north aspects, which leads to lower volumes of water flowing on north aspects of the glacier surface.

Daily melt rates on Fountain Glacier have been measured at 0.06-0.11 m d^{-1} (Whitehead et al., 2014; Bash et al., 2018). Similar melt rates have been measured on other glaciers in the Arctic (e.g. Arnold et al., 2006; Thomson and Copland, 2017), as well as mid-latitude glaciers (e.g. Bash and Marshall, 2014; Fitzpatrick et al., 2017). The ETI models are based on an assumption that solar radiation is the dominant component of glacier surface energy balance (Hock, 2005). Temperature then serves as a proxy for the remaining energy balance terms. Low solar elevations in Arctic summers result in total incoming radiation that is lower than that found at mid-latitude glaciers (Bash and Marshall, 2014; Fitzpatrick et al., 2017; Arnold et al., 2006; Bash et al., 2018). Although solar elevation varies over the course of the day in Arctic summer, 24 hours of daylight dampens diurnal variability in solar radiation as compared to mid-latitudes.

The results of this study suggest that on Fountain Glacier the relative importance of energy flux from water flow is high enough to cause significant errors in the distributed model. On Arctic glaciers, where overall melt rates are similar to mid-latitude glaciers, but solar radiation is relatively stable through the day, other energy contributions to the glacier surface may have more relative importance. This has been noted in other studies (e.g. Hock and Holmgren, 2005), but ETI models continue to be employed for modelling glacier melt regardless of geographic context.

We believe that the relative importance of factors other than solar radiation which are driving melt on Fountain Glacier will have cumulative effects if ETI_{dist} were employed for long term modelling. Although this study looks at a short time frame of only 3 days, weather conditions during the study are similar to those found throughout the ablation season on Fountain Glacier and are likely to be representative of average conditions throughout the season. The high melt rates measured on south aspects and in areas of surface water flow, which are absent in the model, are enough to change the terrain characteristics of the glacier over time. The changes in terrain feed back into melt dynamics related to slope and aspect. The inability of ETI_{dist} to capture higher melt seen on south aspects will fail to reproduce this canyon development.

The availability of high resolution melt measurements now allows for analysis of model performance that is not possible with other methods of measuring melt (i.e. ablation stakes or satellite measurements). Building on previous studies of distributed energy balance models, high resolution distributed melt data may be used to develop more appropriate simplifications for glaciers similar to Fountain Glacier. Asymmetrical canyons such as those found on Fountain Glacier have been noted on 83 other glaciers across the Arctic, including 10 on Bylot Island (St. Germain, 2019). Other studies of glacier terrain characteristics have found that gradual shifts in glacier aspect due to differential melt have important impacts on total glacier mass balance

(Arnold et al., 1996, 2006). This reinforces the importance of developing a model which captures melt driven by both radiation and water flow.

5 Conclusions

We present the first study using high resolution measurements derived from SfM and UAV imagery to assess performance of a distributed ETI. In addition we build on the methods of Rippin et al. (2015) for estimating glacier surface albedo to derive a gridded albedo from the UAV imagery that can be used directly in ETI_{dist}. The model developed in this study was compared directly to AWS measurements and to distributed measurements on a cell by cell basis. The availability of high resolution data revealed patterns in model performance that could not be found with other traditional methods of measuring glacier melt (i.e. ablation stakes or satellite measurements).

The ETI_{dist} exhibits similar performance at the AWS to other implementations of ETI models. In the absence of high resolution distributed data, this model might be applied with confidence across the glacier surface. The bulk performance of the model across the study is also similar to distributed melt measurements, with a median error lower than the measurement uncertainty. However, the range in modelled melt is an order of magnitude lower than that seen in distributed melt measurements. The lower range in modelled melt combined with spatial patterns found in model error, allowed for investigation of sources of model error.

Significant correlation between surface water flow and model error highlighted the important role of water flow in melt dynamics on Fountain Glacier. Energy transfer from water flow in supraglacial streams is known to cause stream incision and was previously noted by Bash et al. (2018) on Fountain Glacier. The role of thin sheet flow on the glacier surface has not been studied previously, although Stevens et al. (2018) investigate near-surface hydrology and the role of kinetic energy in weather crust development. Our results corroborate the important role of kinetic energy in surface hydrology and suggest that on Fountain Glacier energy transfer from water flow is a significant driver of melt.

Given the importance of water flow in the development of canyons on Fountain Glacier and the absence of factors contributing to canyon formation in the ETI model, a model which accounts for water related energy inputs is necessary to effectively capture long term surface evolution on the glacier. Other work has shown the influence of changes in surface slope and aspect on overall glacier mass balance, the relation found in this study between model error and aspect indicates the influence of aspect may be even more pronounced on Fountain Glacier. A model which better reflects the drivers of melt on Fountain Glacier, and potentially similar glaciers across the Arctic, will provide insight into changing melt dynamics in these environments. In future work we hope to extend the time series of melt measurements from UAV imagery and use the distributed dataset to derive a new melt model which captures the melt drivers highlighted in this study.

Author contributions. The study was conceptualized by E.A.B., with supervision from B.J.M. Field data collection was designed and performed by E.A.B., with supervision from B.J.M. E.A.B. developed and implemented models, analysed all outputs, and prepared the manuscript. B.J.M. edited the manuscript and provided feedback on analysis.

Competing interests. The authors have no competing interests.

Acknowledgements. This work was supported by a Natural Sciences and Engineering Research Council Discovery Grant. Field support was provided by the Polar Continental Shelf Project, Parks Canada, Northern Scientific Training Program, and the Arctic Institute of North America. E. Bash was supported by the University of Calgary's Eyes High Recruitment Scholarship. We would like to thank Allison Gunther for fieldwork and technical assistance, as well as Mustafizur Rahman for coding assistance.

References

Arnold, N. S., Willis, I. C., Sharp, M. J., Richard, K. S., and Lawson, W. J.: A distributed surface energy-balance model for a small valley glacier. I. Development and testing for Haut Glacier d'Arolla, Valais, Switzerland, Journal of Glaciology, 42, 77–89, 1996.

Arnold, N. S., Rees, W. G., Hodson, A. J., and Kohler, J.: Topographic controls on the surface energy balance of a high Arctic valley glacier, Journal of Geophysical Research: Earth Surface, 111, 2006.

Avanzi, F., Bianchi, A., Cina, A., De Michele, C., Maschio, P., Pagliari, D., Passoni, D., Pinto, L., Piras, M., and Rossi, L.: Centimetric accuracy in snow depth using unmanned aerial system photogrammetry and a multistation, Remote Sensing, 10, 765, 2018.

Bash, E., Moorman, B., and Gunther, A.: Detecting Short-Term Surface Melt on an Arctic Glacier Using UAV Surveys, Remote Sensing, 10, 1547, 2018.

Bash, E. A. and Marshall, S. J.: Estimation of glacial melt contribution to the Bow River, Alberta, Canada, using a radiation-temperature melt model, Annals of Glaciology, 55, 138–152, 2014.

Bugler, J.: The determination of hourly insolation on an inclined plane using a diffuse irradiance model based on hourly measured global horizontal insolation, Solar energy, 19, 477–491, 1977.

Cook, K. L.: An evaluation of the effectiveness of low-cost UAVs and structure from motion for geomorphic change detection, Geomorphology, 278, 195–208, 2017.

Corripio, J. G.: Snow surface albedo estimation using terrestrial photography, International Journal of Remote Sensing, 25, 5705–5729, 2004.

Fisher, D., Zheng, J., Burgess, D., Zdanowicz, C., Kinnard, C., Sharp, M. J., and Bourgeois, J.: Recent melt rates of Canadian arctic ice caps are the highest in four millennia, Global and Planetary Change, 85, 3–7, 2012.

Fitzpatrick, N., Radić, V., and Menounos, B.: Surface Energy Balance Closure and Turbulent Flux Parameterization on a Mid-Latitude Mountain Glacier, Purcell Mountains, Canada, Frontiers in Earth Science, 5, 67, 2017.

Gardner, A., Moholdt, G., and Wouters, B.: Accelerated contributions of Canada's Baffin and Bylot Island glaciers to sea level rise over the past half century, The Cryosphere, 6, 1103–1125, 2012.

Fountain, A. G. and Walder, J. S.: Water flow through temperate glaciers, Reviews of Geophysics, 36, 299–328, 1998.

Gardner, A. S., Moholdt, G., Wouters, B., Wolken, G. J., Burgess, D. O., Sharp, M. J., Cogley, J. G., Braun, C., and Labine, C.: Sharply increased mass loss from glaciers and ice caps in the Canadian Arctic Archipelago, Nature, 473, 357–360, 2011.

Goswami, D. Y., Kreith, F., and Kreider, J. F.: Principles of solar engineering, CRC Press, 2000.

Hock, R.: A distributed temperature-index ice- and snowmelt model including potential direct solar radiation, Journal of Glaciology, 45, 101–111, 1999.

Hock, R.: Glacier melt: a review of processes and their modelling, Progress in Physical Geography, 29, 362–391, 2005.

Hock, R. and Holmgren, B.: A distributed surface energy-balance model for complex topography and its application to Storglaciären, Sweden, Journal of Glaciology, 51, 25–36, 2005.

Höhle, J. and Höhle, M.: Accuracy assessment of digital elevation models by means of robust statistical methods, ISPRS Journal of Photogrammetry and Remote Sensing, 64, 398–406, 2009.

Irvine-Fynn, T., Barrand, N., Porter, P., Hodson, A., and Murray, T.: Recent High-Arctic glacial sediment redistribution: A process perspective using airborne lidar, Geomorphology, 125, 27–39, 2011.

Irvine-Fynn, T. D., Hanna, E., Barrand, N., Porter, P., Kohler, J., and Hodson, A.: Examination of a physically based, high-resolution, distributed Arctic temperature-index melt model, on Midtre Lovénbreen, Svalbard, Hydrological Processes, 28, 134–149, 2014.

James, M. R. and Robson, S.: Sequential digital elevation models of active lava flows from ground-based stereo time-lapse imagery, ISPRS Journal of Photogrammetry and Remote Sensing, 97, 160–170, 2014.

Lague, D., Brodu, N., and Leroux, J.: Accurate 3D comparison of complex topography with terrestrial laser scanner: application to the Rangitikei canyon (N-Z), ISPRS Journal of Photogrammetry and Remote Sensing, 82, 10–26, 2013.

Lenaerts, J. T., van Angelen, J. H., van den Broeke, M. R., Gardner, A. S., Wouters, B., and van Meijgaard, E.: Irreversible mass loss of Canadian Arctic Archipelago glaciers, Geophysical Research Letters, 40, 870–874, 2013.

Lovitt, J., Rahman, M. M., Saraswati, S., McDermid, G. J., Strack, M., and Xu, B.: UAV Remote Sensing Can Reveal the Effects of Low-Impact Seismic Lines on Surface Morphology, Hydrology, and Methane (CH_4) Release in a Boreal Treed Bog, Journal of Geophysical Research: Biogeosciences, 123, 1117–1129, 2018.

MacDougall, A. H. and Flowers, G. E.: Spatial and temporal transferability of a distributed energy-balance glacier melt model, Journal of Climate, 24, 1480–1498, 2011.

Mair, D., Willis, I., Hubbard, B., Fischer, U., Nienow, P., and Hubbard, A.: Hydrological controls on patterns of surface, internal and basal velocities during three "spring events": Haut Glacier d'Arolla, Switzerland, Journal of Glaciology, 49, 555–567, 2003.

Matthews, T., Hodgkins, R., Wilby, R. L., Guðmundsson, S., Pálsson, F., Björnsson, H., and Carr, S.: Conditioning temperature-index model parameters on synoptic weather types for glacier melt simulations, Hydrological processes, 29, 1027–1045, 2015.

Moorman, B. J.: Glacier-permafrost hydrology interactions, Bylot Island, Canada, in: Proceedings of the 8th International Conference on Permafrost, pp. 783–788, 2003.

Noël, B., van de Berg, W. J., Lhermitte, S., Wouters, B., Schaffer, N., and van den Broeke, M. R.: Six decades of glacial mass loss in the Canadian Arctic Archipelago, Journal of Geophysical Research: Earth Surface, 123, 1430–1449, 2018.

Pellicciotti, F., Brock, B., Strasser, U., Burlando, P., Funk, M., and Corripio, J.: An enhanced temperature-index glacier melt model including the shortwave radiation balance: development and testing for Haut Glacier d'Arolla, Switzerland, Journal of Glaciology, 51, 573–587, 2005.

Radić, V. and Hock, R.: Regionally differentiated contribution of mountain glaciers and ice caps to future sea-level rise, Nature Geoscience, 4, 91–94, 2011.

Rippin, D. M., Pomfret, A., and King, N.: High resolution mapping of supra-glacial drainage pathways reveals link between micro-channel drainage density, surface roughness and surface reflectance, Earth Surface Processes and Landforms, 40, 1279–1290, 2015.

Ryan, J. C., Hubbard, A., Box, J. E., Brough, S., Cameron, K., Cook, J. M., Cooper, M., Doyle, S. H., Edwards, A., Holt, T., Irvine-Fynn, T., Jones, C., Pitcher, L. H., Rennermalm, A. K., Smith, L. C., Stibal, M., and Snooke, N.: Derivation of High Spatial Resolution Albedo from UAV Digital Imagery: Application over the Greenland Ice Sheet, Frontiers in Earth Science, 5, 40, 2017.

Shaw, T. E., Brock, B. W., Fyffe, C. L., Pellicciotti, F., Rutter, N., and Diotri, F.: Air temperature distribution and energy-balance modelling of a debris-covered glacier, Journal of Glaciology, 62, 185–198, 2016.

St. Germain, S.: Studies of supraglacial canyons, personal Communication, 2019.

St. Germain, S. and Moorman, B.: The development of a pulsating supraglacial stream, Annals of Glaciology, 57, 31–38, 2016.

Stevens, I. T., Irvine-Fynn, T. D., Porter, P. R., Cook, J. M., Edwards, A., Smart, M., Moorman, B. J., Hodson, A. J., and Mitchell, A. C.: Near-surface hydraulic conductivity of northern hemisphere glaciers, Hydrological Processes, 32, 850–865, 2018.

Thomson, L. I. and Copland, L.: Multi-decadal reduction in glacier velocities and mechanisms driving deceleration at polythermal White Glacier, Arctic Canada, Journal of Glaciology, 63, 450–463, 2017.

Wake, L. and Marshall, S.: Assessment of current methods of positive degree-day calculation using in situ observations from glaciated regions, Journal of Glaciology, 61, 329–344, 2015.

Watson, C. S., Quincey, D. J., Smith, M. W., Carrivick, J. L., Rowan, A. V., and James, M. R.: Quantifying ice cliff evolution with multi-temporal point clouds on the debris-covered Khumbu Glacier, Nepal, Journal of Glaciology, 63, 823–837, 2017.

WGMS, W.: Fluctuations of Glaciers Database, https://doi.org/10.5904/wgms-fog-2018-06, 2018.

Whitehead, K., Moorman, B., and Wainstein, P.: Measuring daily surface elevation and velocity variations across a polythermal arctic glacier using ground-based photogrammetry, Journal of Glaciology, 60, 1208–1220, 2014.